

RSC Advances



This is an *Accepted Manuscript*, which has been through the Royal Society of Chemistry peer review process and has been accepted for publication.

Accepted Manuscripts are published online shortly after acceptance, before technical editing, formatting and proof reading. Using this free service, authors can make their results available to the community, in citable form, before we publish the edited article. This *Accepted Manuscript* will be replaced by the edited, formatted and paginated article as soon as this is available.

You can find more information about *Accepted Manuscripts* in the [Information for Authors](#).

Please note that technical editing may introduce minor changes to the text and/or graphics, which may alter content. The journal's standard [Terms & Conditions](#) and the [Ethical guidelines](#) still apply. In no event shall the Royal Society of Chemistry be held responsible for any errors or omissions in this *Accepted Manuscript* or any consequences arising from the use of any information it contains.

SERS-active Ag@Au core-shell NPs assemblies for DNA detection

Yuan Zhao^{1,2}, Liqiang Liu¹, Hua Kuang¹, Libing Wang¹, Chuanlai Xu^{1*}

An innovative Raman sensor was developed for DNA detection, based on silver@gold (Ag@Au) core-shell nanoparticles (NPs) assemblies fabricated by polymerase chain reaction (PCR). The combination of exponential amplification by PCR and the amplified Raman signal achieved DNA detection of 11.8 aM.

Numerous studies have been carried out on the surface-enhanced Raman spectroscopy (SERS) of geometry-controlled NPs aggregates.^{1,2} The rationale behind the enhancement of SERS is based on the localized surface plasmon resonance (LSPR) of metallic NPs arising from resonant oscillations of the conducting electrons around NPs.³⁻⁵ When an analyte is localized at a junction between NPs (“hot spot”), an enhancement of the electronic and vibrational spectroscopic signals is observed. In comparison to fluorescence, SERS signals are not only free from oxygen, humidity and foreign species, but exhibit 10-100 times narrower spectral bands and possess higher discrimination due to the molecularly specific fingerprint spectra,⁶ and are a promising alternative for biosensing in diverse surroundings.⁷⁻⁹

Despite the extraordinary limits of detection (LODs) for small organic molecules and ions provided by SERS,¹⁰⁻¹⁴ the quantitative application of ultrasensitive biomacromolecules, particularly related to long DNA detection, are necessary for early disease diagnosis and pharmacogenomics, but have significant challenges in the actual applications: (a) the requirements to label Raman reporters on a DNA probe are complex and time-consuming; (b) the restricted LODs at picomolar, and in some cases, femtomolar levels due to large interparticle gaps (Table 1).^{6, 15-20}

1 The design of an efficient and label-free substrate with a consistently high density of
2 hot-spots is crucial for SERS sensors in sensitive long DNA detection.²¹ Anisotropic NPs of
3 various sizes and shapes have recently been engineered to optimize high electromagnetic fields in
4 a controlled arrangement.²²⁻²⁴ Compared to the widely studied Au NPs,^{25, 26} Ag NPs should be of
5 interest in SERS properties, due to their better plasmonic oscillations at visible frequencies.
6 However, the easy oxidation and toxicity of Ag NPs is an intrinsically challenging problem in
7 actual applications. To satisfy the criteria of large-scale stable electromagnetic enhancement, a
8 stable and biocompatible Au shell was deposited on the surface of Ag NPs assemblies. Au shell
9 deposition takes advantage of the excellent plasmon properties of the Ag core, and directly guides
10 the interparticle distance of NPs and engineers the intensity of electromagnetic fields.

11 Herein, Ag NPs multimers were first assembled by PCR attributing to its advantages of
12 exponential amplification and high specificity benefiting from the heat transfer properties of NPs,
13 as well as its automatic manipulations.²⁷⁻²⁹ The enormous enhancement of the SERS signals for Ag
14 NPs assemblies at the sub-3.7 nm gap was exploited by Au shell deposition at different PCR
15 cycles (Fig. 1). Depending on the exponential amplification of interface-PCR and the amplified
16 SERS signal, we determined the bioanalytical potential of Ag@Au core-shell NPs assemblies,
17 which achieved Raman-signal based attomolar DNA detection. Shell driven strong Raman signals
18 allow the fabrication of label-free and highly reproducible SERS-active materials with reliable
19 nanometer gap sizes for biomacromolecule detection.

20 18.0 ± 2.3 nm Ag NPs were synthesized by the reduction of silver nitrate using sodium
21 borohydride (Fig. S1, ESI[†]).³⁰ Forward primers and reverse primers were respectively modified on
22 the surface of Ag NPs by Ag-SH covalent bonds at a molar ratio of 100:1.^{28, 29} Under optimized
23 amplification conditions, Ag NPs assemblies were prepared using 1.56 pM target templates (Fig.
24 1). From 2 to 5 cycles, Ag NPs oligomers involving dimers, trimers and tetramers were gradually
25 assembled; From 10 to 40 cycles, the degree of NPs assemblies increased, resulting in the
26 formation of large sized multimers (Fig. S2, ESI[†]).²⁸

1 A layer of Au shell was post-deposited on the surface of Ag NPs assemblies by the reduction
2 of H₂AuCl₄ solution to prevent Ag NPs from atmospheric oxidation.¹¹ Bright-field TEM images
3 clearly demonstrated the Ag core and Au shell attributing to their distinct contrast grades (Fig. 2a,
4 insert). With an increase in the number of cycles from 2 to 40, Ag@Au core-shell NPs number of
5 assemblies was systematically increased (Fig. 2). Note that the interface configuration of Ag@Au
6 core-shell NPs was not as smooth as that of Ag NPs and transformed into Au dendrites.³¹ Such
7 branched protrusions enabled Ag@Au core-shell NPs to exhibit extraordinary properties in the
8 intensification of the electromagnetic field.³²⁻³⁴ The interparticle distance between NPs was
9 decreased from 16.5 nm to 3.7 ± 1.0 nm after Au shell deposition and can be employed to obtain
10 large intensifications in SERS (Fig. S3, ESI[†]).³⁵ The underlying shell deposition had a significant
11 influence on the plasmonic properties of the assemblies. Compared to the plasmonic peak at 404
12 nm of single Ag NPs, only 4 nm red shifts were observed for Ag NPs multimers assembled after
13 20 cycles, while a significant red shift of 85 nm for Ag@Au core-shell NPs assemblies was seen in
14 the plasmonic resonance peaks which were determined by the LSPR of the encapsulated Ag core
15 and deposited Au shell (Fig. 3).³⁶ Ag NPs assemblies after Au deposition from 2 to 40 cycles
16 showed distinct plasmon resonance which ranging from 489 nm to 499 nm.

17 Clear evidence of narrow-gap plasmonic coupling of Au and Ag heterogeneous elements in
18 Ag@Au core-shell NPs assemblies prompted us to explore their potential SERS properties. In
19 comparison, SERS signals obtained from 4-NTP and the control groups (0 cycles) were weak (Fig.
20 4a). Ag NPs assemblies showed increased Raman signals, and a Raman shift at 1346 cm⁻¹
21 exhibited the highest intensity (Fig. S4, ESI[†]).^{37, 38} From 2 to 20 cycles, the SERS intensity of Ag
22 NPs assemblies correspondingly increased, which was related to the number of hot spots between
23 the gaps of two NPs with increasing degree of aggregation of the Ag NPs. From 20 to 40 cycles,
24 no obvious increase in Raman signals was observed, but a slight decrease was seen, due to the
25 formation of large aggregates which caused sedimentation and induced instability of the solution.
26 Ag NPs multimers assembled at 20 cycles showed the highest Raman signal, but the intensity was

1 only 1295 due to the large gaps between NPs.^{29, 39} However, Ag NPs assemblies after Au shell
2 deposition exhibited as much as 3 orders of magnitude more intensity than that of pure Ag NPs
3 assemblies and showed 8-fold higher intensity than pure 4-NTP (Fig. 4b). The variation law of
4 Raman intensity at different cycles was similar. Particle structure and interparticle distance
5 markedly affected the “hot spots” between metal nanostructures, which were spatial regions where
6 the electromagnetic field was extremely intense contributing to the plasmon coupling between
7 neighboring NPs.^{35, 40} After Au shell deposition, neighboring NPs were closer and the
8 nanofocusing effect was particularly pronounced originating from strong “hot spots” at their
9 junctions where the electromagnetic field was enormously enhanced, and numerous enhanced
10 regions containing a high density of hot spots. Of particular importance were the slits between
11 small Au tips and Ag cores which acted as novel hot spot generating regions and were favorable
12 for significantly magnifying SERS signals.⁴¹ The highest plasmonic resonance of Ag NPs, the
13 narrow gaps between NPs and the formation of multi-shaped tips on the NPs surface after Au
14 deposition were the deciding factors in the response to SERS signals.^{23, 32, 42} Assemblies at 20
15 cycles was not only more stable than that of 30 and 40 cycles, but contained the maximum NPs
16 number than that of 2, 5 and 10 cycles. Ag@Au core-shell NPs assemblies at 20 cycles possessed
17 the highest density of hot spots and showed the strongest SERS signal which reached up to 3070.

18 A particularly exciting sensing application utilizing the resultant high-efficiency SERS-active
19 Ag@Au core-shell NPs assemblies was exploited. An overview of the experimental data is
20 depicted in Fig. 4. Ag NPs assemblies at 20 PCR cycles after Au deposition exhibited the highest
21 Raman signals, with promising application in the detection of biomolecules. The Raman shift at
22 1346 cm^{-1} was employed as the identification position for the quantitative analysis. As shown in
23 Fig. 5A, the fewer the target templates applied, the smaller the degree of NPs assemblies was
24 formed by PCR. The target concentration was in proportion to the Raman intensity of the
25 assemblies. A standard curve was established between the intensity of the 1346 cm^{-1} peak of
26 4-NTP and the logarithm of DNA concentration in the range of 1.56 pM to 15.6 aM, which

1 exhibited a good correlation ($R^2 = 0.993$) (Fig. 5B). There were no obvious changes in Raman
2 intensity when the DNA concentration was lowered to 1.56 aM and even 156 zM. The LOD was
3 calculated to be 11.8 aM which demonstrated at least a three-fold enhancement of sensitivity
4 compared to previous reports.^{19, 20, 43} It was instructive to evaluate plasmonic-dependent Raman
5 sensors with ultraviolet-visible absorption utilizing the plasmonic properties of NPs. The
6 decreased concentration of target DNA induced a slight blue shift in the ultraviolet-visible
7 absorption spectra (Fig. S5, ESI†).

8 The specificity of the developed method was investigated in the presence of non-target
9 DNA_{EC} (the genome of Escherichia coli). There were no repeated fragments between the genome
10 of Escherichia coli and λ DNA through standard nucleotide BLAST on NCBI. PCR products
11 assembled at 1 fM DNA_{EC} after 20 cycles still showed single NPs dispersity in despite of a few
12 oligomers (Fig. S6, ESI†). No obvious changes of SERS intensity was observed between the PCR
13 products and the control groups. Therefore, strong SERS signal in our study mainly came from the
14 nanostructures assembled by target templates attributing to the specific recognition and
15 amplification between primers and λ DNA, and was correspondingly enhanced with the increasing
16 concentration of λ DNA. The reliability and reproducibility of this method was evaluated by
17 investigating the recovery of six different concentrations of target DNA in spiked detection buffer.
18 The results showed satisfactory recovery in the range of 93.18%-105.24% (Table S1, ESI†). These
19 data demonstrated that this assay would be an accurate and reliable Raman sensor in real sample
20 analysis. The novel combination of the exponential amplification of target DNA by interface-PCR
21 and the amplified intensification of the electromagnetic field after Au shell deposition ensured a
22 shell driven label-free Raman biosensor with high sensitivity and good selectivity for long DNA
23 detection (Table 1).⁴⁴⁻⁴⁶

24 In summary, a Raman signal based attomolar DNA detection platform was developed for the
25 first time. The as-fabricated Ag@Au core-shell NPs assemblies exhibited SERS activities which
26 were superior to commercial SERS substrates in terms of signal intensity and reproducibility. Au

1 deposition not only preserved the strongest plasmonic resonance of Ag NPs, but reduced the gaps
2 between NPs and endowed assemblies with SERS-active tips, which were required to enhance the
3 electromagnetic field. The amplified Raman signal with the aid of exponential amplification by
4 interface-PCR significantly improved the sensitivity of the established Raman sensor with a LOD
5 as low as attomolar level. Post-deposited shell driven amplified SERS signals provide the
6 opportunity to fabricate ideal and reproducible SERS-active substrates, has potential application
7 for the ultrasensitive and may single-molecular level detection of biomacromolecules from
8 biological systems.

9 Acknowledgements

10 This work is financially supported by the Key Programs from MOST 2012BAC01B07.

11 Notes and references

12 ¹State Key Lab of Food Science and Technology, School of Food Science and
13 Technology, Jiangnan University, Wuxi, Jiangsu, 214122, PRC

14 ²The Key Lab of Food Colloids and Biotechnology, Ministry of Education, School of Chemical and Materials
15 Engineering, Jiangnan University, Wuxi, Jiangsu, 214122, PRC

16 †Electronic Supplementary Information (ESI) available: Detail experimental section and additional TEM
17 images and Raman spectra of Ag NPs assemblies, statistical analysis of Au shell thickness. See
18 DOI: 10.1039/c000000x/

19 Email: xcl@jiangnan.edu.cn

20
21 1 N. Gandra, A. Abbas, L. Tian and S. Singamaneni, *Nano letters*, 2012, **12**, 2645-2651.

22 2 A. Lee, G. F. S. Andrade, A. Ahmed, M. L. Souza, N. Coombs, E. Tumarkin, K. Liu, R. Gordon, A. G. Brolo and E.
23 Kumacheva, *J. Am. Chem. Soc.*, 2011, **133**, 7563-7570.

24 3 V. V. Thacker, L. O. Herrmann, D. O. Sigle, T. Zhang, T. Liedl, J. J. Baumberg and U. F. Keyser, *Nat. Commun.*,
25 2014, **5**, 3448.

26 4 J. A. Huang, Y. Q. Zhao, X. J. Zhang, L. F. He, T. L. Wong, Y. S. Chui, W. J. Zhang and S. T. Lee, *Nano Letters*, 2013,
27 **13**, 5039-5045.

28 5 H. Sharma, D. C. Agarwal, A. K. Shukla, D. K. Avasthi and V. D. Vankar, *J. Raman Spectrosc.*, 2012, DOI
29 10.1002/jrs.4136.

30 6 K. Gracie, E. Correa, S. Mabbott, J. A. Dougan, D. Graham, R. Goodacre and K. Faulds, *Chem. Sci.*, 2014, **5**,
31 1030-1040.

32 7 D. van Lierop, I. A. Larmour, K. Faulds and D. Graham, *Anal. Chem.*, 2013, **85**, 1408-1414.

33 8 R. A. Alvarez-Puebla and L. M. Liz-Marzán, *Chem. Soc. Rev.*, 2012, **41**, 43-51.

34 9 Y. Zhao, C. Hao, W. Ma, Q. Yong, W. Yan, H. Kuang, L. Wang and C. Xu, *J. Phys. Chem. C*, 2011, **115**,
35 20134-20140.

36 10 D. K. Lim, K. S. Jeon, H. M. Kim, J. M. Nam and Y. D. Suh, *Nat. Mater.*, 2009, **9**, 60-67.

37 11 D. K. Lim, K. S. Jeon, J. H. Hwang, H. Kim, S. Kwon, Y. D. Suh and J. M. Nam, *Nat. Nanotechnol.*, 2011, **6**,
38 452-460.

39 12 R. Zhang, Y. Zhang, Z. C. Dong, S. Jiang, C. Zhang, L. G. Chen, L. Zhang, Y. Liao, J. Aizpurua, Y. Luo, J. L. Yang
40 and J. G. Hou, *Nature*, 2013, **498**, 82-86.

- 1 13 D. Tsoutsis, L. Guerrini, J. M. Hermida-Ramon, V. Giannini, L. M. Liz-Marzan, A. Wei and R. A. Alvarez-Puebla,
2 *Nanoscale*, 2013, **5**, 5841-5846.
- 3 14 R. A. Alvarez-Puebla and L. M. Liz-Marzan, *Angew Chem Int Ed Engl*, 2012, **51**, 11214-11223.
- 4 15 F. L. Gao, J. P. Lei and H. X. Ju, *Anal. Chem*, 2013, **85**, 11788-11793.
- 5 16 S. He, K.-K. Liu, S. Su, J. Yan, X. Mao, D. Wang, Y. He, L.-J. Li, S. Song and C. Fan, *Anal. Chem*, 2012, **84**,
6 4622-4627.
- 7 17 T. Kang, S. M. Yoo, I. Yoon, S. Y. Lee and B. Kim, *Nano letters*, 2010, **10**, 1189-1193.
- 8 18 Y. C. Cao, *Science*, 2002, **297**, 1536-1540.
- 9 19 R. A. Alvarez-Puebla, E. R. Zubarev, N. A. Kotov and L. M. Liz-Marzán, *Nano Today*, 2012, **7**, 6-9.
- 10 20 K. Faulds, F. McKenzie, W. E. Smith and D. Graham, *Angew. Chem*, 2007, **119**, 1861-1863.
- 11 21 A. Sánchez-Iglesias, P. Aldeanueva-Potel, W. Ni, J. Pérez-Juste, I. Pastoriza-Santos, R. A. Alvarez-Puebla, B. N.
12 Mbenkum and L. M. Liz-Marzán, *Nano Today*, 2010, **5**, 21-27.
- 13 22 Y. H. Zheng, T. Thai, P. Reineck, L. Qiu, Y. M. Guo and U. Bach, *Adv. Func. Mater*, 2013, **23**, 1519-1526.
- 14 23 S. K. Dondapati, T. K. Sau, C. Hrelescu, T. A. Klar, F. D. Stefani and J. Feldmann, *ACS Nano*, 2010, **4**, 6318-6322.
- 15 24 J. M. Romo-Herrera, R. A. Alvarez-Puebla and L. M. Liz-Marzán, *Nanoscale*, 2011, **3**, 1304-1315.
- 16 25 K. Saha, S. S. Agasti, C. Kim, X. Li and V. M. Rotello, *Chem. Rev*, 2012, **112**, 2739-2779.
- 17 26 H. Jans and Q. Huo, *Chem. Soc. Rev*, 2012, **41**, 2849-2866.
- 18 27 H. Kuang, W. Ma, L. Xu, L. Wang and C. Xu, *Acc. Chem. Res.*, 2013, **46**, 2341-2354.
- 19 28 Y. Zhao, L. Xu, H. Kuang, L. Wang and C. Xu, *J. Mater. Chem.*, 2012, **22**, 5574.
- 20 29 Y. Zhao, L. Xu, L. M. Liz-Marzán, H. Kuang, W. Ma, A. Asenjo-García, F. J. García de Abajo, N. A. Kotov, L. Wang
21 and C. Xu, *J. Phys. Chem. Lett.*, 2013, **4**, 641-647.
- 22 30 W. Yan, L. Xu, C. Xu, W. Ma, H. Kuang, L. Wang, and N. A. Kotov, *J. Am. Chem. Soc.*, 2012, **134**, 15114-15121.
- 23 31 H. Zhou, J. P. Kim, J. H. Bahng, N. A. Kotov and J. Lee, *Adv. Funct. Mater*, 2013, **24**, 1439-1448.
- 24 32 M. Yang, R. n. Alvarez-Puebla, H.-S. Kim, P. Aldeanueva-Potel, L. M. Liz-Marzán and N. A. Kotov, *Nano letters*,
25 2010, **10**, 4013-4019.
- 26 33 Y. Zhao, L. Xu, W. Ma, L. Wang, H. Kuang, C. Xu, N. A. Kotov, *Nano Lett.* 2014, **14**, 3908-3913..
- 27 34 Y. Zhao, L. Xu, W. Ma, L. Liu, L. Wang, H. Kuang and C. Xu, *Small*, 2014, DOI: 10.1002/sml. 201401203.
- 28 35 M. Shanthil, R. Thomas, R. Swathi and K. George Thomas, *J. Phys. Chem. Lett.*, 2012, **3**, 1459-1464.
- 29 36 P. P. Patra, G. V. Pavan Kumar, *J. Phys. Chem. Lett.*, 2013, **4**, 1167-1171.
- 30 37 L. Xu, H. Kuang, C. Xu, W. Ma, L. Wang and N. A. Kotov, *J. Am. Chem. Soc.*, 2012, **134**, 1699-1709.
- 31 38 Y. Zhu, H. Kuang, L. Xu, W. Ma, C. Peng, Y. Hua, L. Wang and C. Xu, *J. Mater. Chem.*, 2012, **22**, 2387-2391.
- 32 39 W. Ma, H. Kuang, L. Xu, L. Ding, C. Xu, L. Wang and N. A. Kotov, *Nat. Commun.*, 2013, **4**, 2689.
- 33 40 A. Lombardi, M. P. Grzelczak, A. Crut, P. Maioli, I. Pastoriza-Santos, L. M. Liz-Marzán, N. Del Fatti and F. Vallée,
34 *ACS Nano*, 2013, **7**, 2522-2531.
- 35 41 W. Ma, M. Sun, L. Xu, L. Wang, H. Kuang and C. Xu, *Chem Commun (Camb)*, 2013, **49**, 4989-4991.
- 36 42 C. Hrelescu, T. K. Sau, A. L. Rogach, F. Jäckel, G. Laurent, L. Douillard and F. Charra, *Nano letters*, 2011, **11**,
37 402-407.
- 38 43 R. J. Stokes, A. Macaskill, P. J. Lundahl, W. E. Smith, K. Faulds and D. Graham, *Small*, 2007, **3**, 1593-1601.
- 39 44 D. van Lierop, K. Faulds and D. Graham, *Anal. Chem.*, 2011, **83**, 5817-5821.
- 40 45 D. Graham, D. G. Thompson, W. E. Smith and K. Faulds, *Nat. Nanotech.*, 2008, **3**, 548-551.
- 41 46 Y. He, S. Su, T. Xu, Y. Zhong, J. A. Zapien, J. Li, C. Fan and S.-T. Lee, *Nano Today*, 2011, **6**, 122-130.
- 42
- 43

Captions:

Fig. 1 Schematic illustration of SERS detection of DNA by PCR-based Ag@Au core-shell NPs assemblies.

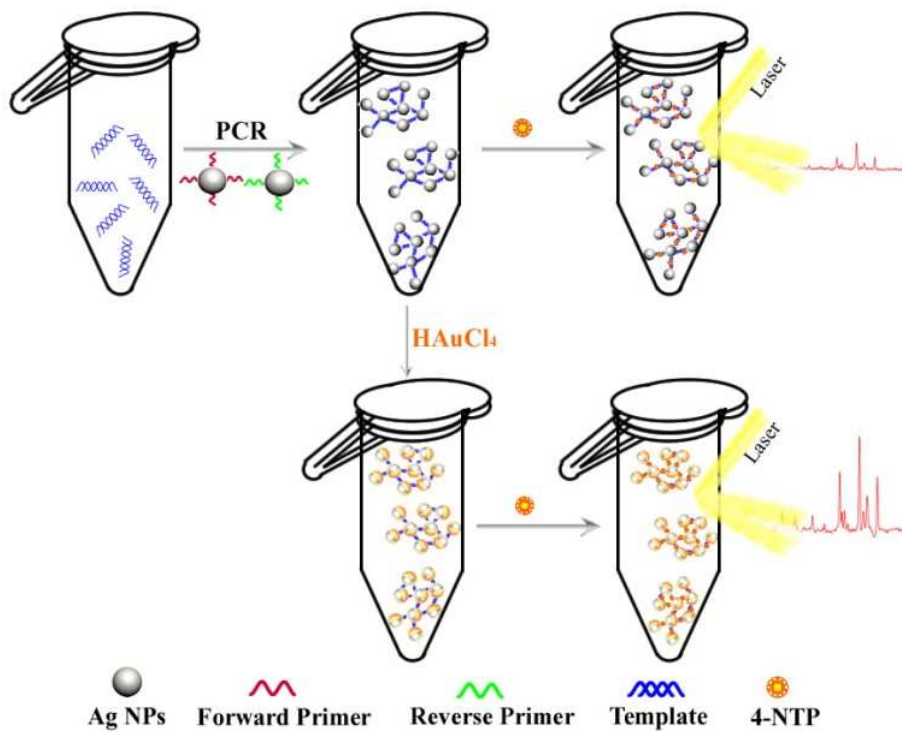
Fig. 2 (a-f) TEM images of Ag NPs assemblies by deposition of HAuCl₄ solution after 2, 5, 10, 20, 30, 40 cycles. Insert in a, the enlarged TEM images of Ag@Au core-shell NPs assemblies after 2 cycles.

Fig. 3 UV-vis spectra of Ag NPs, Au NPs, Ag NPs assemblies, Ag@Au core-shell NPs assemblies after different cycles.

Fig. 4 (a) SERS spectrum of Ag@Au core-shell NPs assemblies after different cycles compared with pure 4-NTP and control groups. (b) Evolution of spectral features of 4-NTP, control groups and Ag@Au core-shell NPs assemblies with increasing cycles.

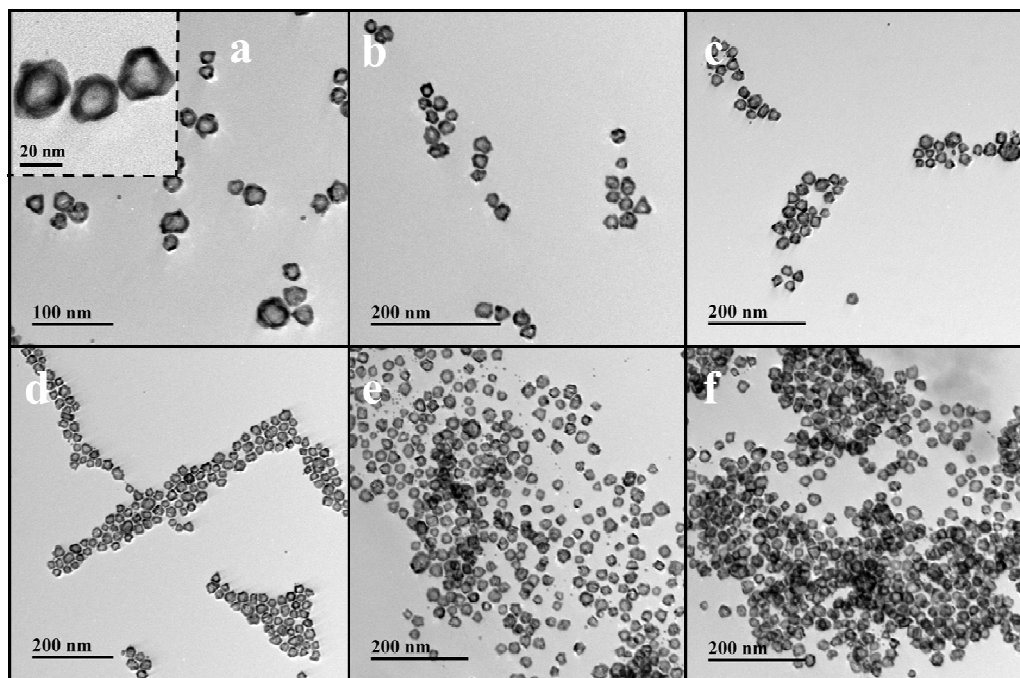
Fig. 5 (a) SERS spectrum of Ag@Au core-shell NPs assemblies at different DNA concentration after 20 cycles. (b) Calibration curves between DNA concentration and Raman intensity of Ag@Au core-shell NPs assemblies. Error bars represented the standard deviation of sample measurements.

Table 1. LODs for SERS based DNA detection by different analytical methods.

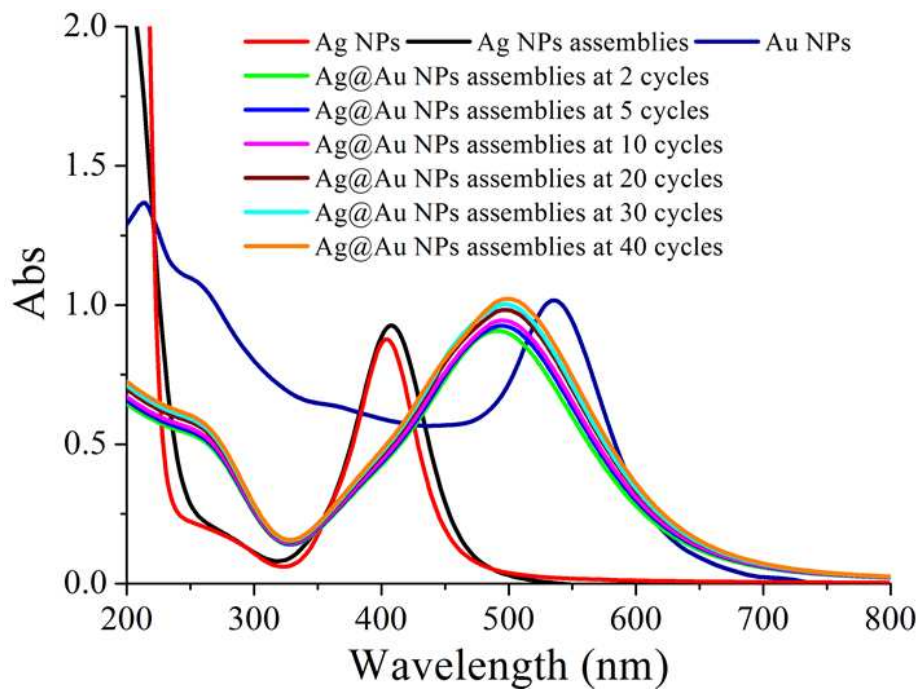


1
2
3
4

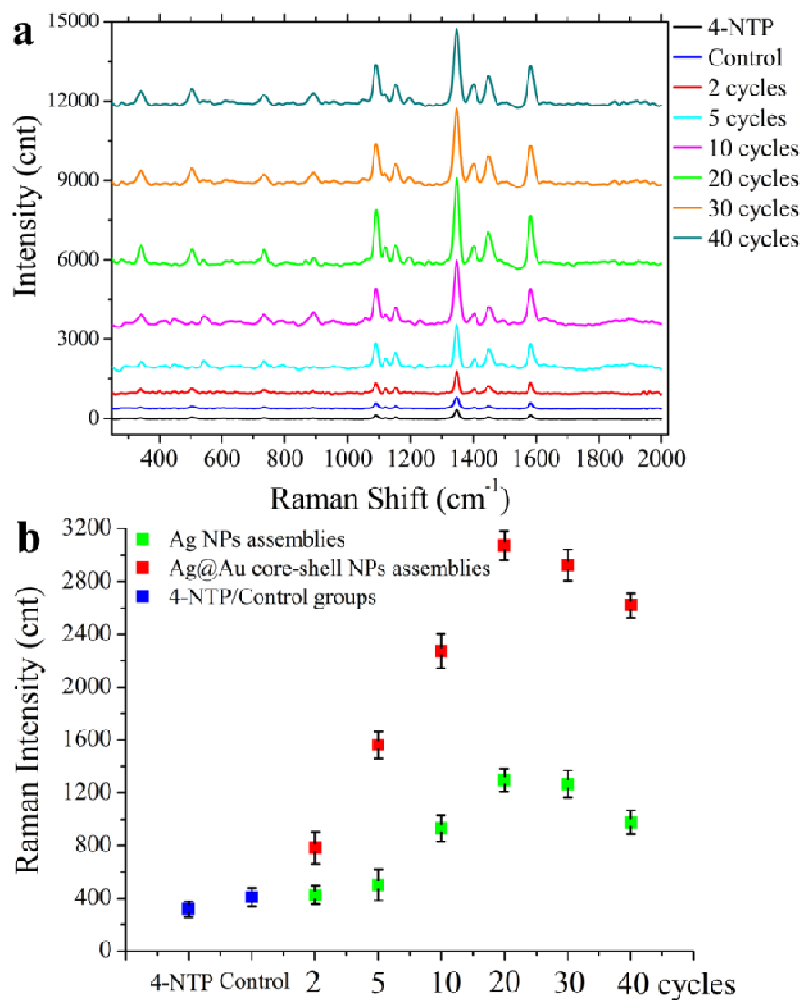
Fig. 1 Schematic illustration of SERS detection of DNA by PCR-based Ag@Au core-shell NPs assemblies.



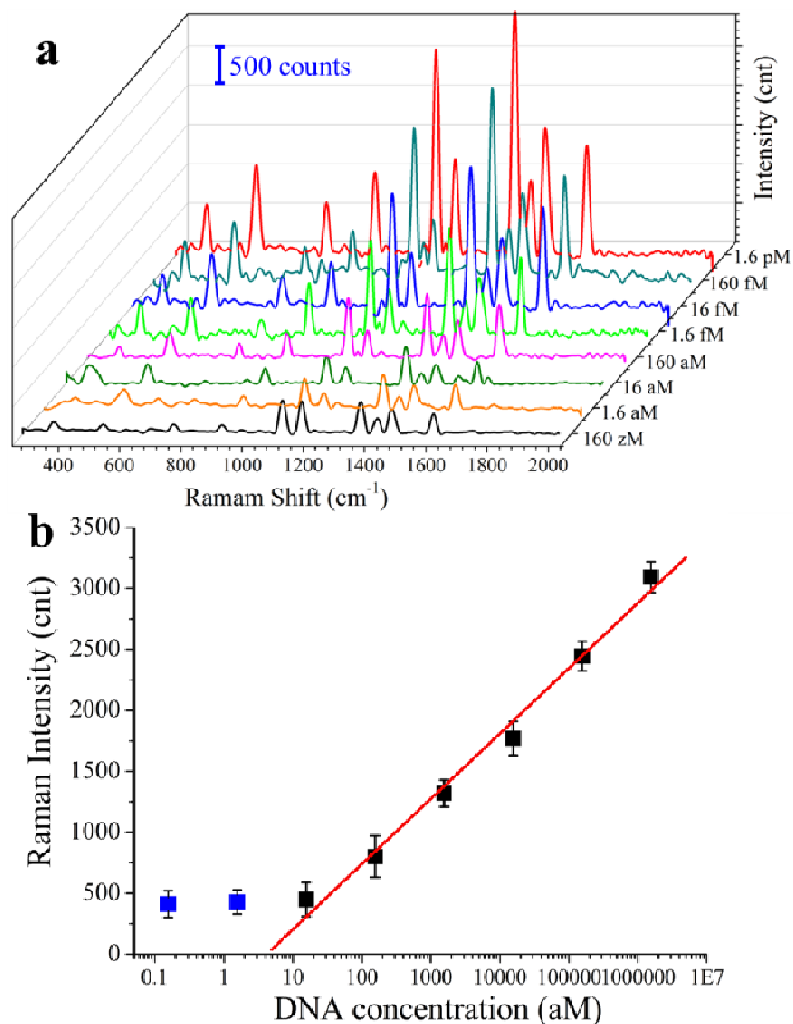
1
2 **Fig. 2** (a-f) TEM images of Ag NPs assemblies by deposition of HAuCl₄ solution after 2, 5, 10, 20,
3 30, 40 cycles. Insert in a, the enlarged TEM images of Ag@Au core-shell NPs assemblies after 2
4 cycles.
5



2
3 **Fig. 3** UV-vis spectra of Ag NPs, Au NPs, Ag NPs assemblies, Ag@Au core-shell NPs assemblies
4 after different cycles.



1
2 **Fig. 4** (a) SERS spectrum of Ag@Au core-shell NPs assemblies after different cycles compared
3 with pure 4-NTP and control groups. (b) Evolution of spectral features of 4-NTP, control groups
4 and Ag@Au core-shell NPs assemblies with increasing cycles.
5

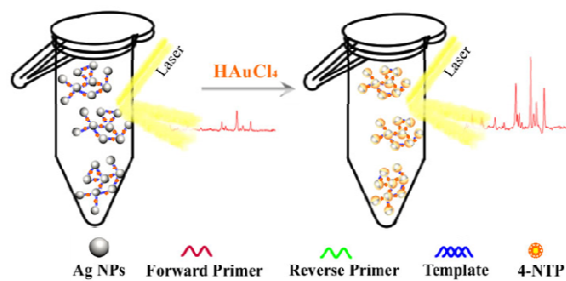


1
2 **Fig. 5** (a) SERS spectrum of Ag@Au core-shell NPs assemblies at different DNA concentration
3 after 20 cycles. (b) Calibration curves between DNA concentration and Raman intensity of
4 Ag@Au core-shell NPs assemblies. Error bars represented the standard deviation of sample
5 measurements.
6
7

1
2**Table 1.** LODs for SERS based DNA detection by different analytical methods.

General Features	Signal	LODs	Refs
Dye-labeled SERS primers	SERS	1 nM	7, 44
Raman reporter dye-coded Ag NPs	SERRS ^a	1.25 nM	45
SERS-active dye labeled DNA probes, Requires lambda exonuclease	SERS	21.7 pM	6
Graphene with in situ grown Au NPs, Reporter-labeled DNA	SERS	10 pM	16
Au NPs-on-Au nanowires, Reporter DNA with Raman dye	SERS	10 pM	17
Hybridization chain reaction coupled with DNA-mediated Ag NPs growth	SERS	3.4 pM	15
Dye-labeled oligonucleotide probe	SERS	750 fM	43
NPs with Raman spectroscopic fingerprints, Raman dye-labeled DNA	SERS	20 fM	18
The adsorption of a colored molecule onto Ag NPs	SERRS	1.17 fM	20
Silicon nanowires with in situ grown Ag NPs, Dye-attached DNA	SERS	1 fM	46

^aSERRS, surface-enhanced resonance Raman scattering



TOC Figure

SERS-active silver@gold (Ag@Au) core-shell nanoparticles (NPs) assemblies were fabricated by polymerase chain reaction (PCR) for the sensitive DNA detection.